Chapter 6

Microstructure and mechanical properties of multiaxially forged Fe-30Mn-9Al-0.8C and Fe-20Mn-10Al-1C low-density steels

6.1 Introduction

In this chapter, Fe-Mn-Al-C low-density steel is deformed using MAF. The microstructural examination is conducted using OM, XRD and EBSD and the evolution of mechanical properties are investigated based on the number of MAF passes. The XRD analysis confirms the refinement of the austenitic phase, indicating a decrease in crystallite size along with an increase in microstrain and dislocation density in the deformed samples. These findings are also supported by EBSD results. MAF leads to an increase in strength and a decrease in ductility. The enhancement in yield strength, ultimate tensile strength and hardness after MAF is due to the combined effects of increased dislocation density, substructure formation, and reduced crystallite size.

6.2 Results and discussion

6.2.1 Multiaxially forged workpiece

SS1 steel workpiece undergoes the MAF process for 5 complete passes before breaking during the 6^{th} pass. In contrast, the SS2 steel workpiece endures only 2 complete passes before breaking during the 3^{rd} pass. Figure 31 illustrates the MAF-processed workpieces of SS1 and SS2 steels, along with the tensile specimens extracted from them.

(a)

(b)

Fig. 31: (a) Tensile sample and forged material after 1 Pass, 3 Pass, and 5 Pass of SS1 steel (b) Tensile sample and forged material after 1 Pass, and 2 Pass of SS2 steel.

6.2.2 Optical microstructure analysis

The SS1 and SS2 steels comprise ferrite and austenite, as discussed in chapter 4. In the SS1 steel composition, approximately 98.5% or more austenite and 1.5% or less ferrite are present, whereas SS2 steel, approximately 95% or more austenite and 5% or less ferrite are present. MAF of these steel workpieces introduce complex stresses into their microstructure due to strain accumulation in the x, y, and z directions during each pass. This increases the dislocation density at the grain boundaries, leading to intersecting deformed grain boundaries and the formation of refined grains after each MAF pass.

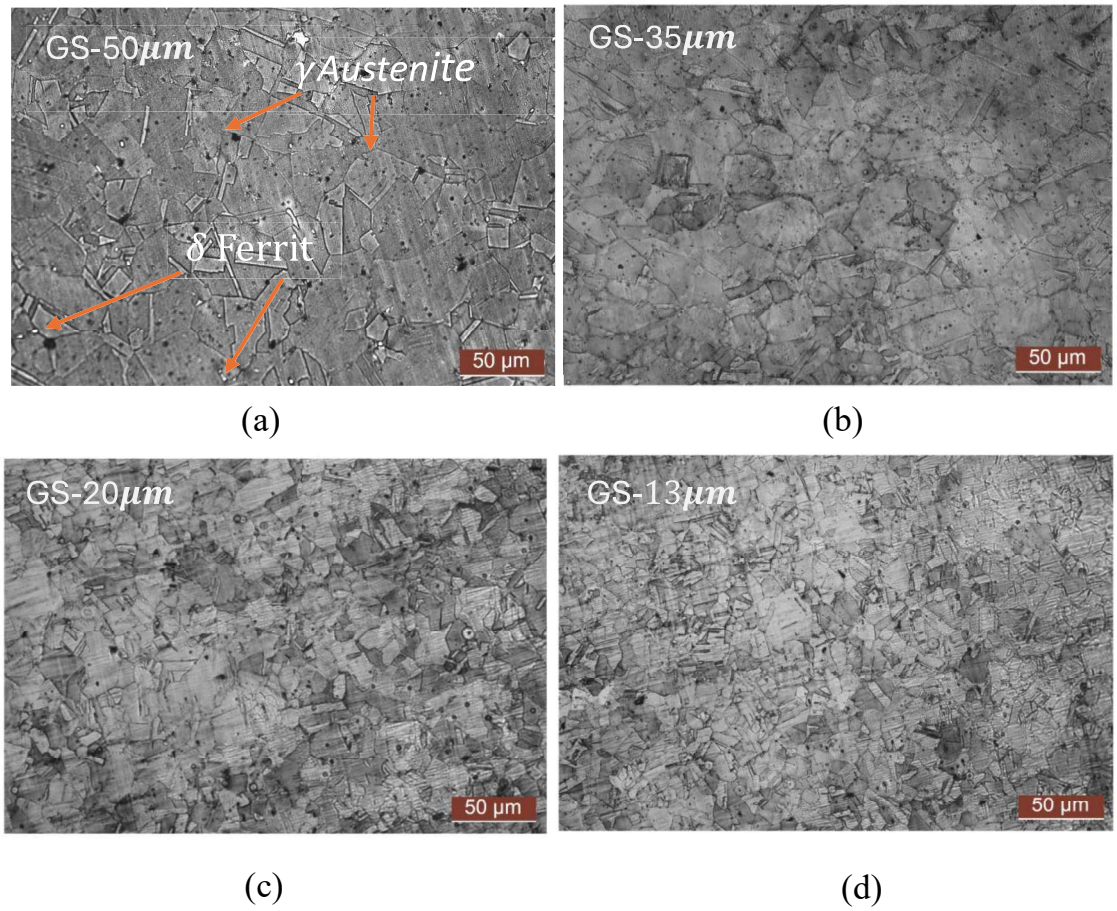

Fig. 32: OM of SS1 Steel (a) MAF-0, (b) MAF-1 and (c) MAF-5.

The average grain size after the MAF-1 of SS1 steel is found to be 35 µm, as shown in Fig. 32b. With more MAF passes, the strain values continue to rise, and the combined effect of continuous effective strain and complex stresses enhances the density of the substructure up to the MAF-5, resulting in finer grains with an average size of 13 µm, as shown in Fig. 32c. This grain size is about one-fourth that of the MAF-0. In the case of SS2 steel, the initial microstructure consists of irregularly sized austenite grains (Fig 33a). Twins are present within the austenite grains, and elongated ferrite phases are located at the boundaries of the austenite phase. After the MAF-1, the average size of the austenite grains is reduced from 80 µm to 66 µm, as shown in Fig. 33b. Some twin boundaries are converted to austenite boundaries, contributing to the formation of uniform austenite grain sizes.

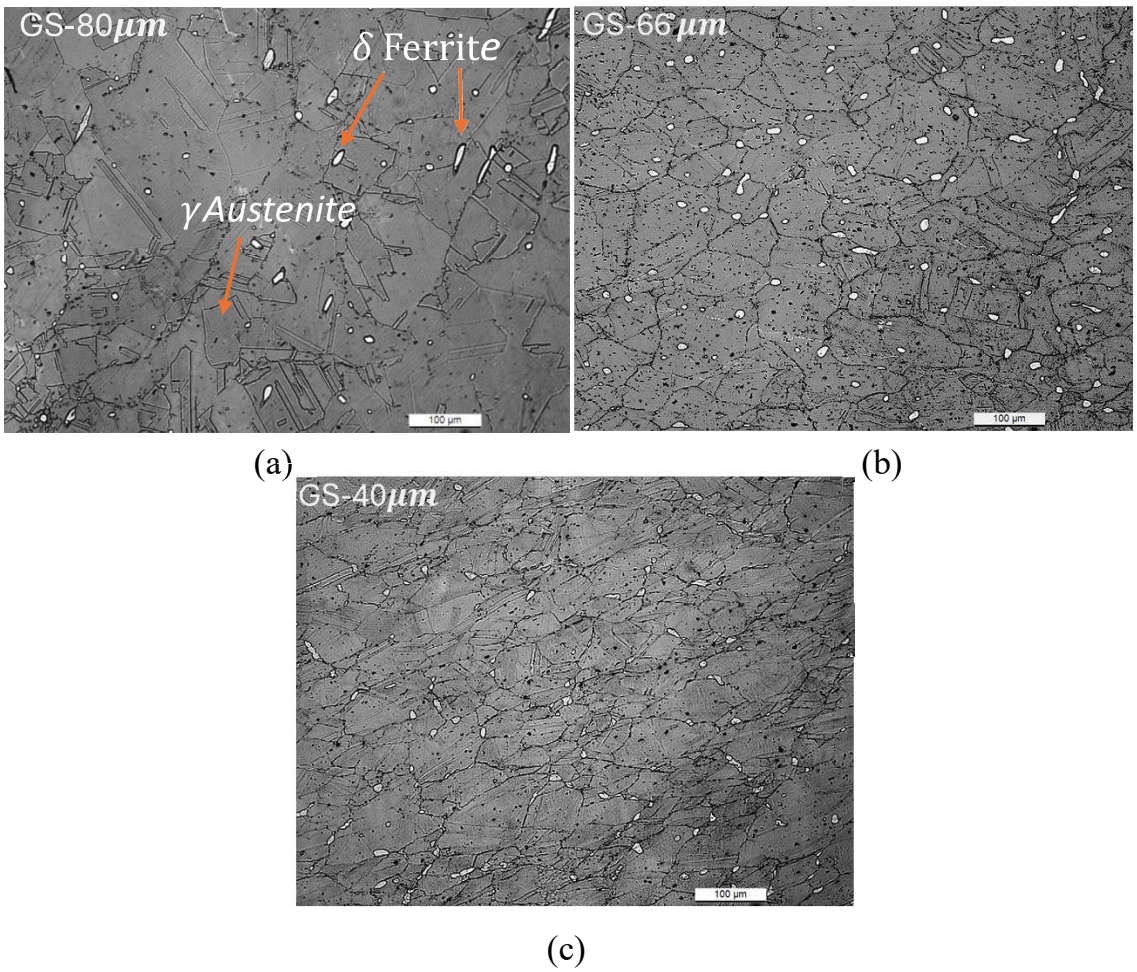

Fig. 33: OM of SS2 steel (a) MAF-0, (b) MAF-1 and (c) MAF-2.

The ferrite grains are also refined and uniformly spread at the austenite boundaries. During the MAF-2, the austenite grains become elongated and further refined to an average size of 40 μm (Fig. 33c), with an increased number of twin boundaries compared to the first pass. The ferrite grains are further reduced and remain uniformly distributed at the austenite boundaries.

6.2.3 XRD analysis

Figure 34a depicts the XRD patterns of SS1 low-density steel and Fig. 34b depicts the XRD patterns of SS2 low-density steel which have undergone MAF passes. Through XRD

analysis, the dislocation density of the MAF specimen is estimated. The examined Fe-Mn-Al-C steels have mostly austenite phase. A notable finding is the change in intensity and broadening of the peaks in the steel specimens as the number of forging passes rises. This phenomenon has been attributed to two primary factors: the refinement of crystallite size and an increase in the lattice strain. The changing of high intensity for (111) plane in SS1 steel to (220) plane of MAF-1 indicates texturing, which may have consequences for the material's characteristics.

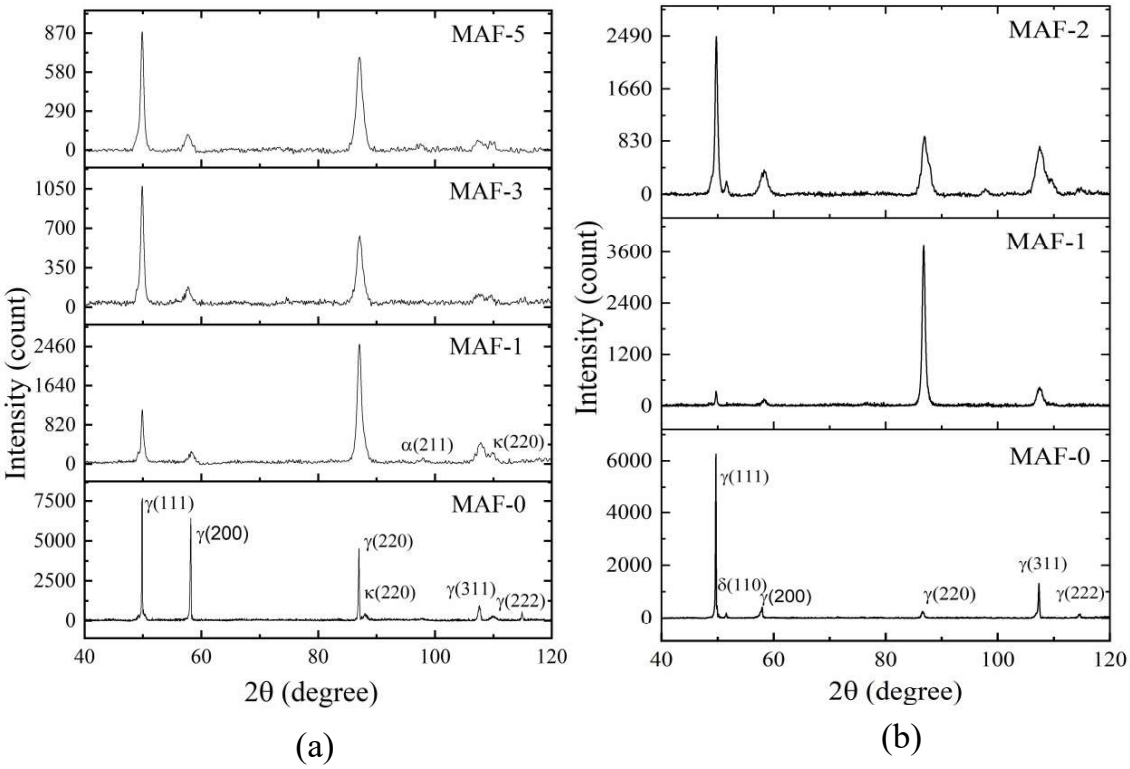

Fig. 34: XRD analysis of (a) SS1, (b) SS2.

The MAF samples exhibit a peak shift towards a lower angle compared to the MAF-0 sample. This shift is attributed to grain refinement in the structure. A slight increase in peak intensity (220) is observed after MAF-5 compared to MAF-3 in SS1 steel and (311) plane after MAF-2 compared to MAF-1 in SS2 steel. This increase is expected due to the dynamic

equilibrium between the formation and annihilation of grains under high strain conditions [177].

Through the study of the average peak broadening of all FCC peaks, lattice microstrain (ϵ) and crystallite size (D) have been determined (values given in Table 11 and Table 12) according to Williamson Hall plot [178]. The value of the Burgers vector, *b*, is calculated to be 0.259 nm. The dislocation densities for the samples are estimated from the Taylors equation.

Table 11: Crystallite size, microstrain, dislocation density for SS1 steel calculated from XRD data.

Sr. no	Grain size (μm)	Volume fraction (%)	Crystallite size (nm)	Microstrain	Dislocation density (m^{-2})
MAF-0	50	γ = 100	61	3.66×10^{-3}	0.79×10^{15}
MAF-1	35	γ = 100	13.4	5.18×10^{-3}	5.57×10^{15}
MAF-3	20	γ = 100	10.87	6.13×10^{-3}	7.5×10^{15}
MAF-5	13	γ = 100	10.12	6.88×10^{-3}	8.98×10^{15}

Table 12: Crystallite size, microstrain, dislocation density for SS2 steel calculated from XRD data.

Sr. no	Grain size (μm)	Volume fraction (%)	Crystallite size (nm)	Micro strain	Dislocation density (m^{-2})
Initial	80	γ = 95, δ = 5	44.9	2.296×10^{-3}	0.68×10^{14}
MAF-1	66	γ = 94.5, δ = 5.5	20.3	3.353×10^{-3}	2.2×10^{14}
MAF-2	40	γ = 95.1, δ = 4.9	10.54	7.107×10^{-3}	8.97×10^{14}

In SS1 steel, the dislocation density is continuously increasing during the MAF. The average dislocation density is increased from 0.11×10^{15} m^{-2} for MAF-0 to 4.8×10^{15} m^{-2} for MAF-5. In SS2 steel also, the dislocation density is continuously increasing during the MAF. The average dislocation density is increased from 0.68×10^{14} m^{-2} for MAF-0 to 8.97

x 10^{14} m^{-2} for MAF-2. A similar method is used by Sarkar et al. [179] to determine the dislocation density of equal channel angular treated IF steel at strains of 1.15 and 4.6, and they have reported the corresponding values as 3.6 x 10^{14} m^{-2} and 6.88 x 10^{14} m^{-2}, respectively. Odnobokova et al. [180] examined the effects of cold rolling and multidirectional forging on 316L steel. They have reported that dislocation density increases from 2 x 10^{15} m^{-2} to 4 x 10^{15} m^{-2} for cold rolling and from 6 x 10^{15} m^{-2} to 7.5 x 10^{15} m^{-2} for multidirectional forging when the total strain value reaches 4. This demonstrates a trend of increasing dislocation densities with plastic strain during cold working processes. SS2 steel exhibits a similar trend during the MAF process. However, in SS1 steel, with increasing plastic strain, the dislocation density initially increases, reaching a maximum, after which the rate of increase slows down. This suggests that dislocations are rearranging at higher strain levels during the MAF process. The distinct behavior observed in SS1 steel may be attributed to the fact that it has undergone MAF to a greater strain. The dislocation density reaches a saturation point at large strain levels because the processes of dislocation annihilation and subgrain boundary formation balance out the generation of new dislocations. Beyond this point, increasing strain does not lead to a significant rise in dislocation density, as the microstructure has already adapted to the deformation by forming subgrain boundaries [67], [181].

6.2.4 EBSD analysis of Fe-30Mn-9Al-0.8C (SS1) low-density steel

The image quality maps (Figs. 35a-d) superimposed with low angle (<15°) and high angle (>15°) grain boundaries represented by green and red colors, respectively. IQ map of MAF-0 sample (Fig. 35a) show low amount (0.367) of low angle boundaries. After MAF-1 (Fig. 35b), the low angle boundaries fraction sharply increases to 0.903. After MAF-3 (Fig. 35c), the low angle boundaries fraction decreases to 0.75. But after MAF-5 (Fig. 35d), it increases to 0.824. The solutionised and WQ material (SS1) has high fraction of high angle

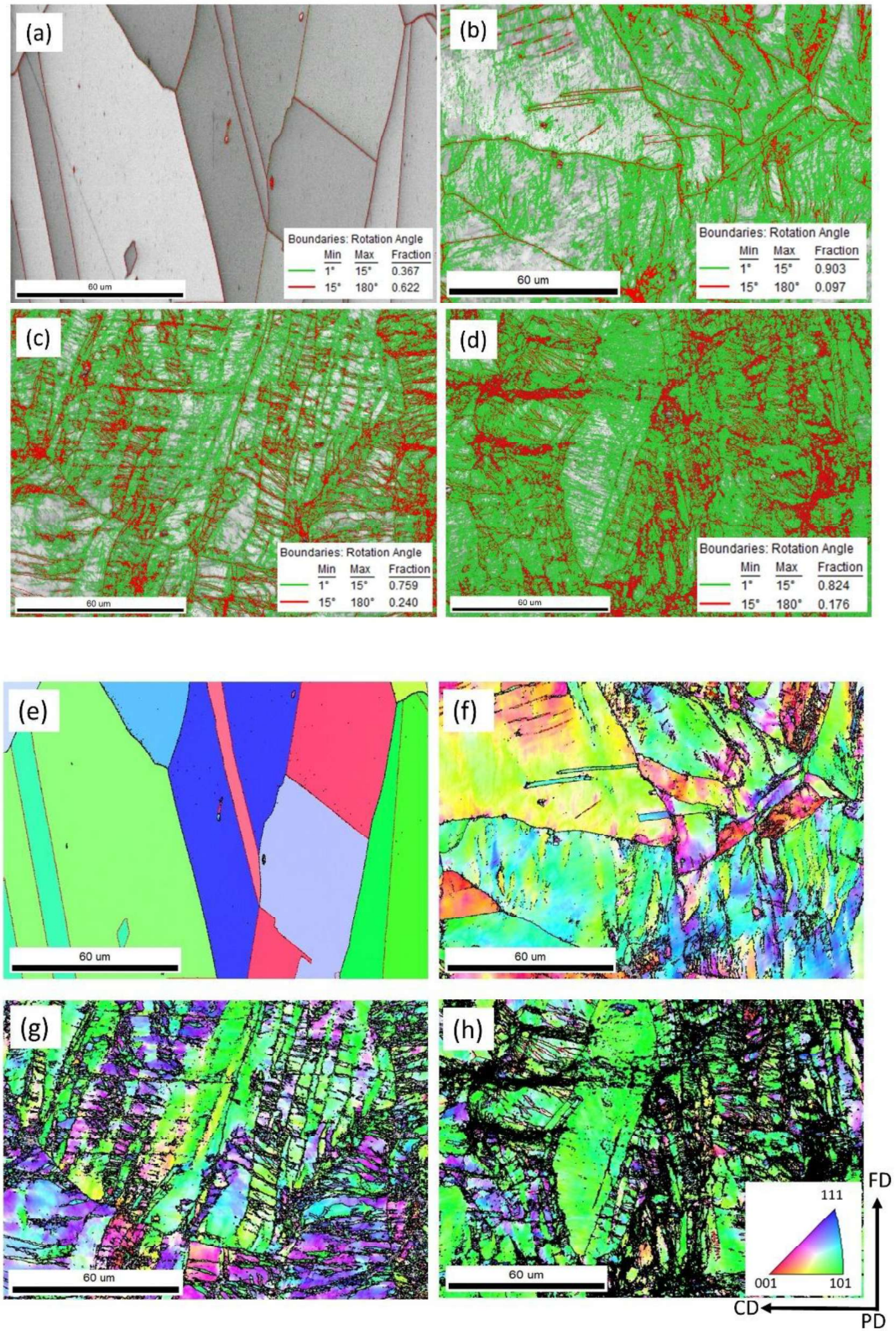
(a)
Boundaries: Rotation Angle
Min Max Fraction
1° 15° 0.367
15° 180° 0.622
60 um
(b)
Boundaries: Rotation Angle
Min Max Fraction
1° 15° 0.903
15° 180° 0.097
60 um
(c)
Boundaries: Rotation Angle
Min Max Fraction
1° 15° 0.759
15° 180° 0.240
60 um
(d)
Boundaries: Rotation Angle
Min Max Fraction
1° 15° 0.824
15° 180° 0.176
60 um
(e)
60 um
(f)
60 um
(g)
60 um
(h)
60 um
111
001 101
FD
CD
PD

Fig. 35: continued..

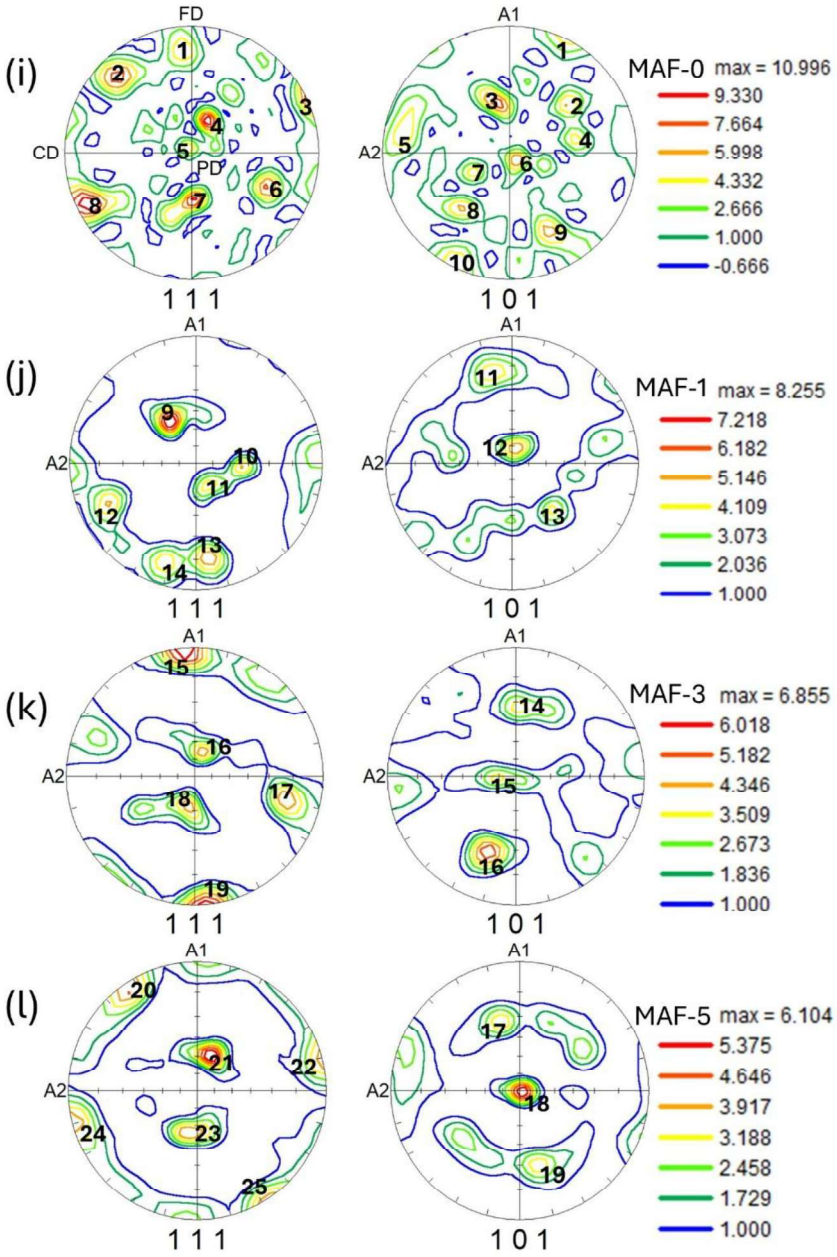

Fig. 35: Image quality maps (a) MAF-0, (b) MAF-1, (c) MAF-3, and (d) MAF-5. Green and red lines are superimposed for boundaries having misorientation angles of 1°-15° and 15°-180°, respectively. Inverse pole figure maps of normal or pressing direction in the present cases for (e) MAF-0, (f) MAF-1, (g) MAF-3, and (h) MAF-5. Color coded scale of IPF for austenite is superimposed on Fig. h with sample reference axis. 111 and 101 Pole figures of (i) MAF-0, (j) MAF-1, (k) MAF-3, and (l) MAF-5.

boundaries and low fraction of low angle boundaries (Fig. 35a). With one pass of MAF, low angle grain boundary fraction increases rapidly but with completion of one cycle (three pass) some of low angle grain boundary are converted to high angle grain boundary. But again, on five passes, between the one cycle and two cycle the low angle grain boundary are increased.

Figures 35(e-h) display inverse pole figure maps of normal direction (pressing direction). Figure 35e shows the IPF maps of MAF-0. The sample is highly textured. [101] direction of high significant number of grains (>50%) is parallel to pressing direction. [111] direction of significant amount of grain (>20%) is parallel to pressing direction. [001] direction of other significant amount of grain (>10%) is parallel to pressing direction. Therefore, the solutionised and WQ is strongly textured (Fig. 35e). The IPF map of MAF-1(Fig. 35f) indicates development of many more texture components with reduced volume fraction. On further MAF for three passes (Fig.35g), the number of orientations increases but their intensity decreases. After five passes of MAF the IPF (Fig. 35h) shows further increase in orientation with reduced intensity.

The 111 and 101 pole figures of MAF materials are analysed (Fig. 35(i-l)). 111 and 101 pole figures of MAF-0 (Fig. 35i) display texture components 1 to 8 and 1 to 10 having maximum texture intensity of 10.996. After one pass of MAF (MAF-1) texture intensities are reduced. The 111 and 101 pole figures of MAF-1 (Fig. 35j) display texture components 9 to 14 and 11 to 13 having maximum texture intensity of 8.255. After three passes of MAF (MAF-3) the texture intensities are further reduced. The 111 and 101 pole figures of MAF-3 (Fig. 35k) display texture components 15 to 19 and 14 to 16 having maximum texture intensity of 6.855. After five passes of MAF (MAF-5) the texture intensities reduced. The 111 and 101 pole figures of MAF-5 (Fig. 35l) display texture components 20 to 25 and 17 to 19 having maximum texture intensity of 6.104. Continuing MAF reduces texture

intensity, and it approaches towards randomization. Therefore, the analysis of pole figure data also supports inverse pole figure data.

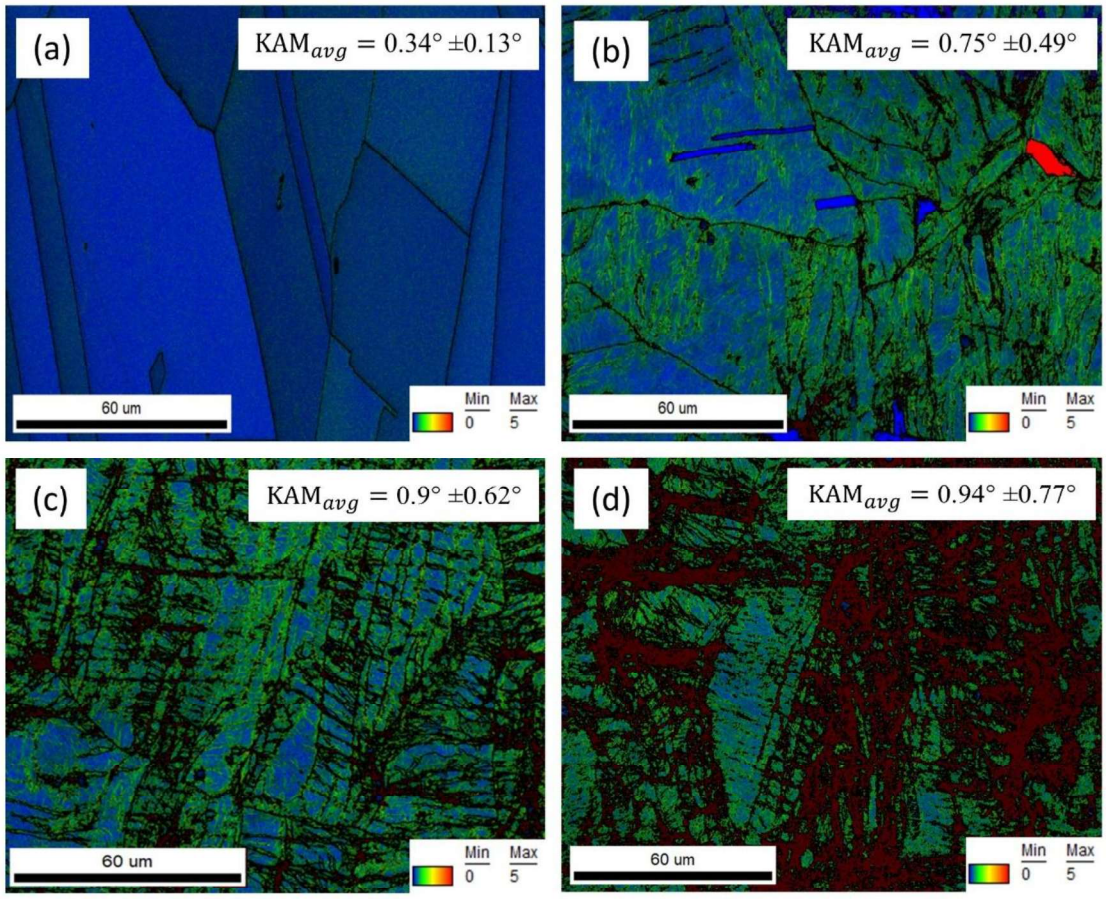

Fig. 36: KAM map (Unique color map) (a) MAF-0, (b) MAF-1, (c) MAF-3, and (d) MAF-5.

Figure 36 shows the KAM maps for MAF samples. Initially MAF-0 contain 60% high angle boundary with reports KAM values of 0.335° ±0.13°. This indicates minimal plastic deformation in the material persisting even after solution annealing (which can be seen in Fig. 36a, the blue color represents low strain). Figure 36b illustrates the KAM map after a single forging pass. °. After one pass of MAF, the amount of high angle grain boundary reduces drastically to 6.1 % which results in KAM values sharply to 0.75° ±0.49°. Figure

36c represents the KAM map after three passes. After three passes of MAF, the high angle grain boundary marginally increases to 12% but the KAM modifies to 0.9 ± 0.62°. This indicates a higher level of plastic deformation. After 5 passes of MAF, the high angle grain boundary increases to 13% but the KAM values increase to 1.07° ± 0.77°. Ideally with increasing high angle grain boundary, the KAM values should decrease but, in the present, result the std. deviation in KAM values is very much comparable to the average value. Due to high amount of error or std deviation the decreasing KAM value with increasing marginal amount of grain boundary is not reflected, which is absorbed in error limit.

6.2.4 Mechanical property

6.2.4.1 Strength

The engineering stress-strain curves of SS1steel are shown in Fig. 37 for MAF-0, MAF-1, MAF-3, and MAF-5. The solutionised and WQ coarse-grained low-density steel (MAF-0) displays lowest yield strength of 380 MPa. On MAF for 1 pass, yield strength increases drastically, i.e. by three times to 1040 MPa. The enhancement in strength is mainly due to increase in dislocation density to 4.53 x 10^{15} m^{-2} which is about 41 times the solutionised material and a marginal refinement in grain size from 50 μm to 35 μm. On further MAF for 3 passes, yield strength increases to 1279 MPa. Here, again the dislocation density of MAF-3 is 4.93 x 10^{15} m^{-2} which is 45 times that of MAF-0 and again grain size reduces to 20 μm. After 5 passes of MAF, yield strength increases to 1528 MPa. The dislocation density of MAF-5 is measured to be 4.88 x 10^{15} m^{-2} which is about 44 times to that the solutionised material and the grains refine from 50 μm to the size of 13 μm. The ultimate tensile strength of coarse-grained solutionised material displays 762 MPa. The highest amount of work hardening of 392 MPa is calculated for the solutionised material. On MAF, as dislocation density increases, the amount of work hardening decreases. As a result,

MAF-1 gives ultimate tensile strength of 1368 MPa and amount of work hardening of 328 MPa. On further MAF for 3 passes, the ultimate tensile strength increases to 1415 MPa and the amount of work hardening decreases to 126 MPa and after 5 passes it reduces to only 20 MPa. In this condition ultimate tensile strength (1548 MPa) and yield strength (1528 MPa) are very close.

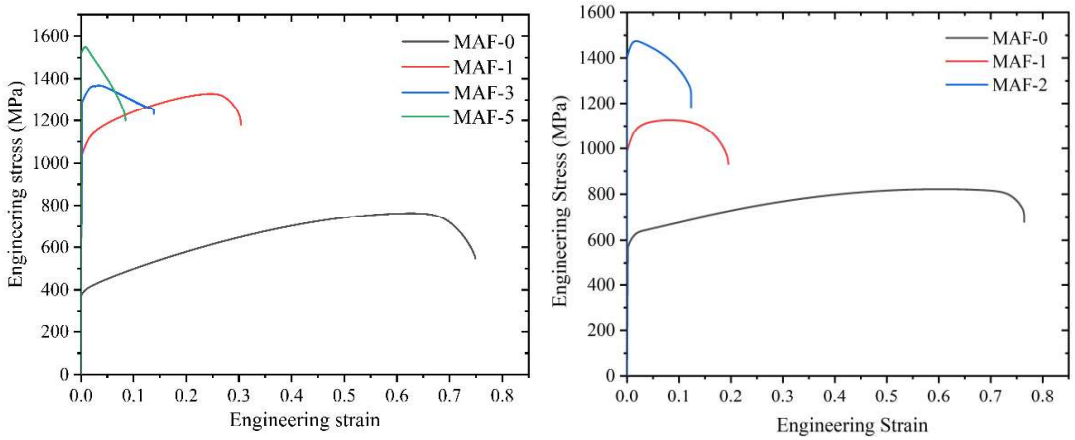

(a) (b)

Fig. 37: Engineering stress-strain plots after different MAF passes of (a) SS1 and (b)SS2 steels.

Table 13: Tensile properties of SS1 low-density steel.

No. of Pass	YS (MPa)	UTS (MPa)	UE (%)	TE (%)	Hardness (HV)
MAF-0	380±12	762±19	64±1.2	74±1.8	230±10
MAF-1	1040±55	1368±42	26±1.7	30±1.85	409±08
MAF-3	1289±72	1415±84	3±0.7	13.7±0.75	530±12
MAF-5	1528±67	1548±102	0.8±0.2	8±1.2	574±16

Table 14: Tensile properties of SS2 low-density steel.

No. of Pass	YS (MPa)	UTS (MPa)	UE (%)	TE (%)	Hardness (HV)
MAF-0	570±15	821±23	60±0.7	76±1.9	200±12

MAF-1	1000±41	1127±53	4±1.2	21±2.1	390±6
MAF-2	1419±65	1474±72	2.2±0.9	13±1.3	520±16

The stress-strain curves of SS2 steel are shown in Fig. 37b at MAF-0, MAF-1, and MAF-2. The MAF-0 displays lowest yield strength of 570 MPa. On MAF for 1 pass, yield strength increases drastically to 1000 MPa. The enhancement in strength is mainly due to increase in dislocation density to 2.2 x 10^{14} m^{-2} which is about 3 times the solutionised material and a marginal refinement in grain size from 80 μm to 66 μm. On further MAF for 2 passes, yield strength increases to 1419 MPa. Here, again the dislocation density of MAF-3 is 8.97x10^{14} m^{-2} which is 14 times that of solutionised material and the grain size reduces to 40 μm. The ultimate tensile strength of coarse-grained solutionised material displays 821 MPa. The highest amount of work hardening of 231 MPa is calculated for the solutionised material. On MAF, as dislocation density increases, the amount of work hardening decreases. As a result, MAF-1 gives ultimate tensile strength of 1124 MPa and amount of work hardening of 127 MPa. On further MAF for 2 passes, the ultimate tensile strength increases to 1474 MPa and the amount of work hardening decreases to 55 MPa.

Miura et al. successfully performed MAF on titanium alloy at room temperature, followed by additional cold rolling. Their study revealed a significant increase in the tensile strength from 710 MPa to 930 MPa attributed to increasing cumulative strain mainly by mechanical twinning and kinking [182]. According to Li et al., the yield strength of the steels dramatically increases by roughly 120-190% compared to the as-received sample after dynamic plastic deformation processing. The combination of dislocation and grain boundary strengthening is responsible for the significant improvement [183]. The primary factors for improving mechanical characteristics like ultimate tensile strength and yield

strength include increased microstrain, and lower crystallite size which in turn results in higher average dislocation density at low-temperature deformation [184-186]. The systematic increase in strength is due to increase in dislocation density, deformation twinning, refinement in grain size, decrease in crystallite size and enhancement in microstrain.

An increase in strength is a commonly desired and observed feature of metals processed by SPD techniques. In the present work, as the number of strain steps increases, the dislocation density is expected to rise, leading to the formation of substructures. The increase in strain leads to the formation of sub-grains, characterized by low angle boundaries, as evidenced by the EBSD results in Fig 35. With further increases in the number of strain steps, the fraction of high angle boundaries also increases. Therefore, the observed increase in strength aligns with expectations, as strength should increase with decreasing grain size according to the Hall–Petch relationship. The presence of substructures and dislocations in ultrafine-grained materials indicates that residual work hardening has contributed, albeit to a lesser extent, to the improvement in strength [187]. Additionally, with an increasing number of strain steps in SS2, the ferrite is fragmented, refined, and finely dispersed within the austenite matrix. These finer grains with high angle boundaries, along with the formed sub-grains (low angle boundaries) and submicron-sized ferrite particles, hinder dislocation movement, resulting in higher strength values. This is evident in the increased ultimate tensile strength values.

6.2.4.1 Ductility

Initially, at MAF-0, the SS1 steel possesses very high total elongation of 75% and uniform elongation (UE) of 63% while SS2 steel possess total elongation of 76 % and uniform elongation of 60%. This is due to relatively strain-free or low dislocation density, low microstrain and high work hardening ability. But, when the sample is multiaxially forged

at imposed strain of 0.46, the total elongation of low-density steels decreases drastically to 30% and 21%, respectively, due to increase in microstrain but rapid enhancement in dislocation density under which material loses its work hardening ability. As a result, the difference between yield strength and ultimate tensile strength decreases from that of solutionised material. On further imposed strain of 1.4 by MAF, the total elongation reduces to 13.7% or uniform elongation reduces to 3%. SS1 steel completes 5 passes with imposed equivalent strain of 2.3, the material gains very high dislocation density, and microstrain. As a result, material loses its work hardening ability to only 20 MPa because of which uniform elongation and total elongation decrease to very low value of 0.8% and 8%, respectively. SS2 steel completes only 2 passes with imposed strain of 0.92. The material undergoes grain refinement in both austenite and ferrite phases, and the dislocation density increases. Consequently, the material's work hardening ability reduces to only 55 MPa, leading to a significant decrease in uniform elongation and total elongation to 2% and 13%, respectively.

One notable aspect of ultrafine-grained steels is their relatively low tensile ductility at room temperature, particularly in terms of uniform elongation, compared to their coarse-grained counterparts. This phenomenon is also observed in the current study. The data presented in Fig. 37 indicate that grain refinement leads to a reduction in work hardening. The decrease in tensile ductility at temperatures below recrystallization for the multiaxially forged steel can be explained as follows:

Firstly, dynamic recovery acts as a softening mechanism that can reduce the apparent work hardening rate. During tensile deformation, dislocations carrying intragranular strain become trapped at grain boundaries. In ultrafine-grained steels, the dynamics of recovery involve the migration of these trapped lattice dislocations into the grain boundaries [188-190]. This change in dislocation density during dynamic recovery, characterized by the

movement of trapped lattice dislocations into grain boundaries, has been extensively studied by Park et al. [191]. The authors calculated the approximate times for dislocations to spread into grain boundaries. Their results show that, for ultrafine-grained steels, this spreading time is shorter than the deformation time during a tensile test. This rapid decrease in dislocation density prevents significant accumulation of dislocations within the grains, leading to reduced work hardening compared to steels with larger grain sizes.

Secondly, the decrease in tensile ductility can be attributed to plastic instabilities that lead to necking due to excessive localized deformation. The initiation of necking in a tensile test is described by the Considère criterion, $\Theta = d\sigma/d\varepsilon$ [192]. According to this criterion, when the slope of the true stress-true strain curve (work hardening rate), $\Theta = d\sigma/d\varepsilon$, equals the true stress, σ, uniform deformation ceases and necking begins. As previously mentioned, ultrafine grains significantly increase the flow stress of steels, particularly in the early stages of plastic deformation. However, the present work also shows that grain refinement reduces the work hardening capacity. Consequently, plastic instability (necking) occurs early during tensile testing, resulting in limited uniform elongation in ultrafine-grained steels.

6.2.5 Hardness

Vickers hardness is measured for all the multiaxial forged samples. The variation in Vickers hardness number for SS1 and SS2 steels with the number of passes of multiaxially forged specimens for cumulative strain is shown in Fig. 38. Similar to the microstructure evaluation, where grain refinement is observed from zero to the final pass, a corresponding pattern is observed in hardness, which has increased rapidly from the initial to the final pass.

For SS1 steel, at lower strain levels, Vickers hardness has increased significantly with MAF strain, from 230 VHN at an effective strain of 0 to 409 VHN at an effective strain of 0.46. Subsequently, a marginal increment in hardness has been observed, ranging from 409 VHN to 530 VHN as the effective strain has increased from 0.46 to 1.38, and from 530 VHN to 574 VHN as the effective strain has increased from 1.38 to 2.3. In the case of SS2 steel, after the first pass of MAF, the hardness has nearly doubled from approximately 200 VHN to 390 VHN. During the second pass, an increase in hardness to around 520 VHN has been observed, albeit at a slower rate.

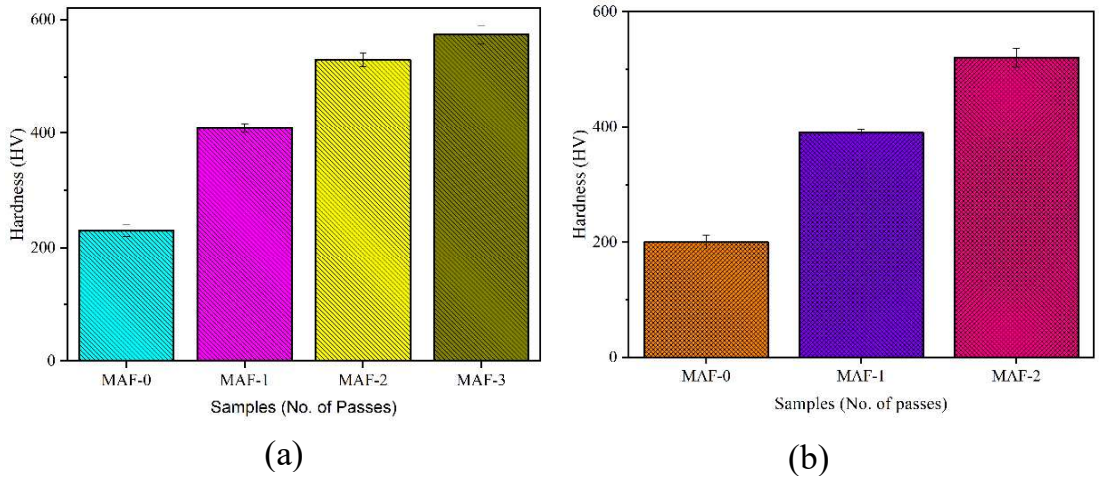

Fig. 38: Average Vickers hardness for (a) SS1, (b) SS2 steels at different MAF passes.

In the case of SS2 steel, after the first pass of MAF, the hardness has nearly doubled from approximately 200 VHN to 390 VHN. During the second pass, an increase in hardness to around 520 VHN has been observed, albeit at a slower rate.

The significant increase in hardness during the first pass is mainly attributed to the substantial rise in dislocation density and reduction in grain size. This increase in hardness correlates with the enhancement of strength after MAF processing. Due to grain refinement,

the effect of grain size on strength follows the classical Hall-Petch relation, where strength increases as grain size decreases. This is because a smaller grain size reduces the number of dislocations in pile-ups before they encounter an obstacle, leading to a much smaller stress concentration in the next grain [193-194]. As a result, a much larger applied stress is required for slip to pass through the boundary in fine-grained materials [195]. The reduced grain size leads to a significant increase in grain boundary area, which hampers dislocation mobility, thereby necessitating a large stress to overcome the obstacle.

As stated earlier, at higher strain levels, the rate of increase in dislocation density decreases, while the rate of refinement increases. Similarly, hardness values show a diminishing rate of increase at higher strain levels. This is attributed to a competition between the softening effect from the reduction in dislocation density and the strengthening due to grain refinement. As the dislocation density decreases, the material's strength diminishes because dislocation movement is less impeded by grain boundaries, which act as barriers. Additionally, it is observed from the graph that the ultimate tensile strength increases while elongation decreases with an increase in MAF passes.

6.2.6 Fractography

The SEM fractographs obtained from tensile samples of SS1 and SS2 steels and after subjected to warm MAF passes are shown in Fig. 39. Figures 39a and 39c show the fracture surface of a sample SS1 and SS2, repectivly subjected at MAF-0 condition. The fracture surfaces of both steels are characterized by large and deep dimples, indicating a ductile failure mode. This dimpled morphology corresponds to the high amount of energy that has been utilised to produce these fracture surfaces and thus the ductility observed in SS1 and SS2 steels exhibit 75% and 76% ductility, respectively.

As the number of MAF passes is increased in both steels, the prevalence of dimpled features is decreased, while cleavage features and dimple rupture become more prominent. These

mixed-mode fracture characteristics are clearly evident in Fig. 39b for MAF-5 in SS1 and 39d for MAF-2 in SS2 steel, respectively, and correspond with the observed reduction in ductility, specifically the percentage of uniform strain to failure 0.3% and 2.2 % respectivly, during the tensile testing. It's clear that the dimple size in the MAF-5 sample of SS1 (Fig. 39b) is reduced to 4 µm, compared to 50 µm in the MAF-0 sample (Fig. 39a). This consistent reduction in dimple size across the MAF samples likely results from microstructural refinement caused by SPD, as noted in previous studies. In sample SS2, the dimple size does not vary significantly, but the deeper dimples in MAF-0 have become shallower, and dimple rupture is more prominent. This could lead to reduced ductility in the MAF-2 tensile sample.

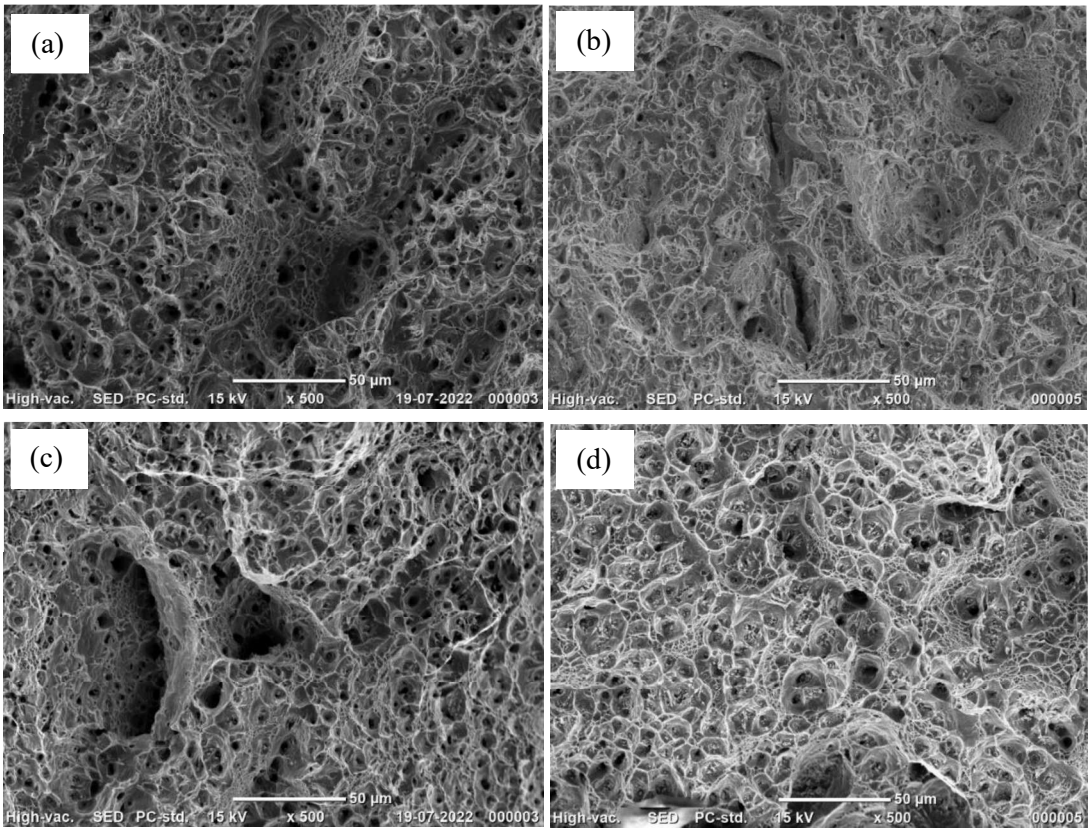

Fig. 39: Fracture morphology of (a) MAF-0, (b) MAF-5 of SS1 steel and (c) MAF-0, (d) MAF-2 of SS2 steel.

6.3 Conclusions

The main objective of the present chapter is to thoroughly understand the microstructural changes of SS1 and SS2 low-density steels during its MAF and their relationships to the material's mechanical properties. Based on results of the present study, the major conclusions are summarized as follows:

- MAF up to an equivalent strain of 2.3 reduces the grain size of SS1 steel from 50 μm to 13 μm, while in SS2 steel, the grain size is reduced from 80 μm to 40 μm.
- After completing five passes of MAF, the yield strength of SS1 steel increases by 4 times, while SS2 steel shows a 2.4-fold increase in yield strength.
- The tensile strength of SS1 steel increases significantly from 762 MPa to 1548 MPa after MAF, though this is accompanied by a drastic reduction in ductility, dropping from 64% to 0.8%. Similarly, in SS2 steel, the tensile strength increases from 821 MPa to 1474 MPa after two passes of MAF, with a corresponding decrease in ductility from 60% to 2%.
- At the initial passes, most of grain boundaries are low angle boundaries. With increasing amount of strain low angle boundaries get converted to high angle boundaries.
- Dislocations density increases up to 3 passes then dislocation recovery is observed for SS1.